Acta Astronautica 213 (2023) 567–577

Contents lists available at ScienceDirect

Acta Astronautica

journal homepage: www.elsevier.com/locate/actaastro

Research paper

Folding, stowage, and deployment of composite thin-walled lenticular tubes

Ruiwen Guo [a,1], Xin Jin [b,1], Qilong Jia [a,c], Xiaofei Ma [b], Ning An [a,d,e,*], Jinxiong Zhou [a]

[a] State Key Laboratory for Strength and Vibration of Mechanical Structures and School of Aerospace, Xi'an Jiaotong University, Xi'an 710049, People's Republic of China
[b] Xi'an Institute of Space Radio Technology, Xi'an 710100, People's Republic of China
[c] Jeatron Technology Co., Ltd., Shanghai, 201800, People's Republic of China
[d] School of Aeronautics and Astronautics, Sichuan University, Chengdu 610065, People's Republic of China
[e] State Key Laboratory of Structural Analysis for Industrial Equipment, Dalian University of Technology, Dalian 116024, People's Republic of China

ARTICLE INFO

Dataset link: https://github.com/XJTU-Zhou-group/CTLT-Dynamic-Deployment

Keywords:
Space deployable structures
Composite thin-walled lenticular tube (CTLT)
Long-term storage
Deployment dynamics
Finite element analysis

ABSTRACT

Composite thin-walled lenticular tube (CTLT) is a lightweight foldable and deployable structural material that enables large-scale deployable mechanisms for various space missions. A key step toward the structural design of CTLT is to understand its folding, stowage, and deployment behaviors. This work presents an integrated experimental and numerical investigation of the dynamic deployment behavior of CTLT that wraps around a central hub, with emphasis on the effect of long-term storage. A two-meter-long CTLT prototype was manufactured, and a gravity compensation system was designed and built for the on-ground dynamic deployment experiments. The deployment experiments were performed on the CTLT prototype both before and after it had been stowed for extended storage periods. The results indicate that after being stowed for 6 and 10.5 months the CTLT is deployed slower and the deployment time increases by 8.2% and 15.0%, respectively. Furthermore, a high-fidelity numerical model was constructed using the explicit dynamic finite element method, where the CTLT was modeled as a deformable part and the folding/deployment mechanisms were modeled as rigid bodies to perform the folding, stowage, and deployment simulations. The long-term storage effect was accounted for in the numerical analyses with the use of a viscoelastic fiber-reinforced composite material model, and a good agreement has been achieved between the experimental and numerical results.

1. Introduction

Lightweight space deployable structures with high storage ratios have become cutting-edge topics in space science and technology due to the rapidly growing use of small spacecraft missions for space exploration [1,2]. Composite thin-walled lenticular tube (CTLT) is a collapsible, rollable and deployable tubular boom made of thin-ply carbon fiber-reinforced composite laminates, which has been considered as one of the most promising structural materials for a wide range of deployable and reconfigurable mechanisms including solar sails [3–7], large membrane reflectors [8–12], rib-mesh antennas [13–15], and morphing wings [16]. The CTLT usually experiences three stages during its service life: folding, stowage, and deployment. Taking the CTLT assembling in a wrapped-rib antenna for example, (*i*), before launch, it is flattened and wrapped around a central hub to reduce volume; (*ii*), during launch and transportation to orbit, it is fastened by a locking device and is stowed in the folded state. This period can last for several months to years, which is referred to as the stowage period; and (*iii*), after reaching the orbit, the CTLT deploys itself by releasing the stored strain energy, which drives related components such as solar sails and antenna reflectors into their functional state.

One basic and crucial step towards designing CTLT is to characterize its folding, stowage, and deployment performance. Various experimental procedures have been proposed for this purpose over the past years. Chu et al. [17] proposed a retractable/deployable mechanism design that is driven by a motor cooperating with reactive springs for folding a space probe of a microsatellite. Chen et al. [18] developed a test setup that employs a scroll tube and a guide wheel to perform wrapping experiments of CTLT specimens by measuring the strain and wrapping moment. Bai et al. [19,20] designed and manufactured a coiling machine that includes a central driving roller, several constraint shafts, torque sensors, and frame structures and is able to drive and record the flattening and coiling deformation of CTLT. Researchers from the German Aerospace Center (DLR) proposed a unifying mechanism for the deployment of the boom as well as solar sail which uses an electric

* Corresponding author at: School of Aeronautics and Astronautics, Sichuan University, Chengdu 610065, People's Republic of China.
E-mail addresses: maxf041600@sina.com (X. Ma), anning@scu.edu.cn (N. An).
[1] These authors contributed equally to this study.

https://doi.org/10.1016/j.actaastro.2023.09.034
Received 3 June 2023; Received in revised form 1 September 2023; Accepted 20 September 2023
Available online 25 September 2023

motor to control the deployment of four CTLT booms and sail segments, and a brake mechanism was taken to prevent uncontrolled dynamic deployment of the booms and sails [21]. Firth et al. [22,23] developed an unpowered and motorless mechanism to control the deployment of CTLT. The deployment was driven by releasing the stored strain energy, while a single roller pressed against the coiled CTLT with enough force to prevent premature unwinding, and a rotary damper was used to limit the deployment speed.

It should be noted that most of the above-mentioned folding, coiling, and deployment mechanisms are designed to produce a steady and controlled deformation process of CTLT, which mimics the deployment of CTLTs in solar sail and membrane antenna systems. On the other hand, for other space deployable mechanisms such as the wrapped-rib antenna, the deployment of CTLT is a highly dynamic transient process where the strain energy stored in the deformed CTLT ribs will be released very rapidly without any external control and the system is expected to be deployed in less than a few seconds. Such dynamic deployment behavior of CTLT remains largely unexplored. The challenge stems from the fact that in the quite short deployment period, CTLT undergoes a significant shape change from the fully stowed state to the fully deployed state. It is non-trivial to develop a gravity compensation system for on-ground dynamic deployment tests of CTLT. Recently, Okuizumi et al. [24] conducted free deployment tests without gravity compensation of CTLT supported with a spring root hinge to investigate the dynamic deployment and vibration behaviors. A 0.6-meter-long CTLT was found to be self-deployed in 2.67 s. It was observed in the experiments that the CTLT tends to deform downward due to gravity when the root of the boom is not yet expanded. Therefore, it is vital to develop a gravity compensation system for performing the dynamic deployment tests of CTLTs on the ground. Many previous studies for the dynamic deployment tests of other types of stored strain energy deployable booms provide insights into the design and implementation of gravity offloading systems. The methods commonly used to eliminate gravity effects for on-ground tests can be classified as physical methods (drop towers or parabolic flight [8,25]), pneumatic (air cushion or air bearings [26]), buoyancy techniques (water floats or helium balloons [27,28]), and mechanical methods (suspension system with elements like cables, strings, pulleys, trolleys, rails or springs [29]). Mallikarachchi et al. [30] developed a gravity offloading system for the dynamic deployment tests of the composite tape-spring hinge (CTSH), where a string was used with one end attached to the outer surface of the tube, and the other end was run over a pulley directly above the center of the CTSH and terminated at a fixed point. Mallol et al. [31] performed dynamic deployment tests on a bistable composite boom suspended in two different gravity offloading systems. The three localized masses of the deployable system could be suspended either by using a two-point string-spring assembly or by using a single point with strings and two soft springs. In this work, the Helium balloon gravity compensation method will be adopted, which has been proven effective for gravity compensation for light-weight structures including CTLTs and solar sails [28].

Another obstacle in characterizing the deployment dynamics of CTLT is the relaxation of stored strain energy during long-time storage. As has been described above, the CTLT would be stowed in the coiled state for a long stowage period before being sent to orbit and deployed. During long-time storage, CTLT is subjected to a constant folded deformation, and stress relaxation is inevitable due to the intrinsic viscoelasticity of matrix resin of composite materials. The stress relaxation leads to a decrease of strain energy stored in the deformation and finally produces an unfavorable impact on the deployment performance of CTLT [32,33]. A number of multiscale modeling approaches of fiber-reinforced viscoelastic composites have been proposed to understand the long-term stowage effects on the deployment dynamics of composite deployable structures, and numerical tools have also been developed and implemented [34–37]. Kwok et al. [36] proposed a general-purpose finite element model that efficiently predicts the deployment performance of plain-weave composite tape-spring shells that are deployed after being held folded for a given period of time. The method was then extended to study the creep recovery of CTLT as well as the recovery behavior of a composite thin-shell deployable reflector antenna [38,39]. A user-friendly micromechanics analysis plug-in tool, *Viscoelastic RVE Calculator*, has been developed within the ABAQUS/CAE environment to rapidly estimate the effective orthotropic viscoelastic properties of unidirectional composites by taking as input the microstructure geometry as well as the known properties of fibers and matrix. The accuracy of the plug-in was validated by comparing its predictions to numerical and experimental results taken from the literature [37,40]. Very recently, Deng et al. [41] applied the method to simulate the effect of storage time and temperature on the deployment dynamics of CTLT and found that the deployment of CTLT becomes slower after being stored for a longer time at a higher temperature, but did not perform experiments to prove it.

In this work, a combination of experiments and simulations is used to investigate the folding, stowage, and deployment behaviors of CTLT. A 2-meter-long CTLT was firstly wrapped around a central hub, and the subsequent deployment was triggered and powered merely by the release of stored strain energy. Helium-filled balloons were used for gravity compensation, and a high-speed camera was used to monitor and record the deformation snapshots of the CTLT during the dynamic deployment process. In order to study the effect of strain energy relaxation caused by long-term stowage, the CTLT was also tested after being held fully wrapped for two given stowage periods of 6 and 10.5 months. In addition, a high-fidelity explicit dynamic finite element model was built to analyze the deformation of the CTLT during the whole process of folding, stowage, and deployment process, and a good correlation between experiments and simulations was achieved.

The rest of the paper is organized as follows. Section 2 presents the manufacturing process and material characterization of CTLT, as well as the development of the gravity compensation system for dynamic deployment testing. Section 3 introduces the numerical model that is used to simulate the folding, stowage, and deployment behaviors of CTLT. The experimental and numerical results are presented and compared in Section 4. Finally, discussions and conclusions are given in Section 5

2. Experiments

2.1. Material and specimens

Fig. 1 schematizes a CTLT boom that is partially coiled around a cylindrical hub. The CTLT considered here consists of two thin-walled Ω−shaped composite shells which are bonded together along the end edges, forming a lenticular cross-section. Each Ω−shaped cross-section is comprised of four circular arcs of radius $r = 15$ mm subtending an angle of $\theta = 45°$, two bonded webs of width $w = 15$ mm, and a straight segment of height $h = 9.6$ mm. The longitudinal length of the CTLT is $L = 2000$ mm and the radius of the hub is $R = 200$ mm. Each Ω−shaped shell of CTLT was manufactured from unidirectional carbon fiber/epoxy prepregs of thickness 0.04 mm and density 1.43 g/cm^3 (T700/Epoxy, Harbin FRP Institute, China). The composite layup is denoted as $[0°, 0°, 90°]_S$, representing a symmetric laminate comprising six plies, where the 0° direction aligns with the longitudinal axis of the CTLT.

The unidirectional composite lamina is considered as a linear elastic and transversely isotropic material and the properties were experimentally measured by performing standard mechanical tests. The carbon fiber and epoxy matrix are both assumed as linear elastic and isotropic materials, and the fibers are assumed periodically spaced in a hexagonal array in the matrix. The properties of fiber and matrix were then determined reversely from the lamina properties by trial-and-error simulations performed with a previously developed ABAQUS plug-in *Viscoelastic RVE Calculator* [37]. The fiber volume fraction was

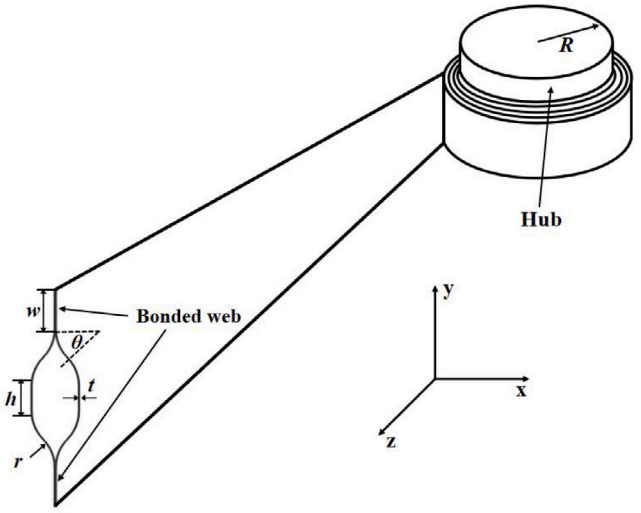

Fig. 1. CTLT partially coiled around a cylindrical hub.

Table 1
Material properties of the constituents and the unidirectional composite lamina T700/Epoxy.

Properties	E_1 [GPa]	E_2 [GPa]	ν_{12}	G_{12} [GPa]	G_{23} [GPa]
T700 fiber	230	–	0.33	–	–
Epoxy matrix	2.38	–	0.30	–	–
T700/Epoxy lamina	137.99	8.71	0.32	3.50	3.21

Table 2
Strength parameters for the unidirectional lamina T700/Epoxy.

Property	Value
Ultimate longitudinal tensile strength, X_t [MPa]	2329.91
Ultimate longitudinal compressive strength, X_c [MPa]	1091.80
Ultimate transverse tensile strength, Y_t [MPa]	129.05
Ultimate transverse compressive strength, Y_c [MPa]	226.32
Ultimate in-plane shear strength, S_{12} [MPa]	253.76

computed to be 60% and the mechanical properties of the constituents and the unidirectional composite lamina were determined as listed in Table 1. In addition, the strength parameters of the unidirectional lamina were also determined through tests and are provided in Table 2 for reference in case of failure analysis.

Having determined the properties of fiber and matrix, we then use *Viscoelastic RVE Calculator* to calculate the relaxed properties for the composite lamina after being stowed for a given period. In these calculations, it was assumed that the elastic modulus of fiber remains unchanged, while the elastic modulus of matrix reduces by a certain amount. Table 3 summarizes the effective lamina properties of T700/Epoxy at different relaxation levels of the matrix. Each set of the lamina properties is related to a distinct virtual temperature, and then the change of material properties will be simulated by inducing a change in the virtual temperature in the simulations. T_0 corresponds to the initial properties of the lamina without being stowed, and T_1, T_2, T_3, T_4, and T_5 correspond to the relaxed properties of the lamina when the elastic modulus of the epoxy matrix reduces by 10%, 20%, 30%, 40%, 50%, respectively.

Fig. 2 illustrates the fabrication process of the CTLT. Only one mold, made from Chinese standard 45 steel, was used due to the inherent symmetry of the CTLT. The initial step involved applying a uniform layer of mold release agent onto the mold's surface, followed by a polishing procedure. Subsequently, the prepreg material was cut and layered on the mold according to the predetermined lay-up design. After all layers had been laid, the mold was packaged in a vacuum bag, and a roller was employed to firmly press the layers together,

Table 3
Lamina properties of T700/Epoxy at different relaxation levels of the matrix.

Properties	E_1 [GPa]	E_2 [GPa]	ν_{12}	G_{12} [GPa]	G_{23} [GPa]
T_0	137.99	8.71	0.32	3.50	3.21
T_1	137.90	7.87	0.32	3.16	2.90
T_2	137.81	7.02	0.32	2.82	2.59
T_3	137.71	6.16	0.32	2.48	2.27
T_4	137.61	5.30	0.32	2.13	1.96
T_5	137.52	4.43	0.32	1.78	1.64

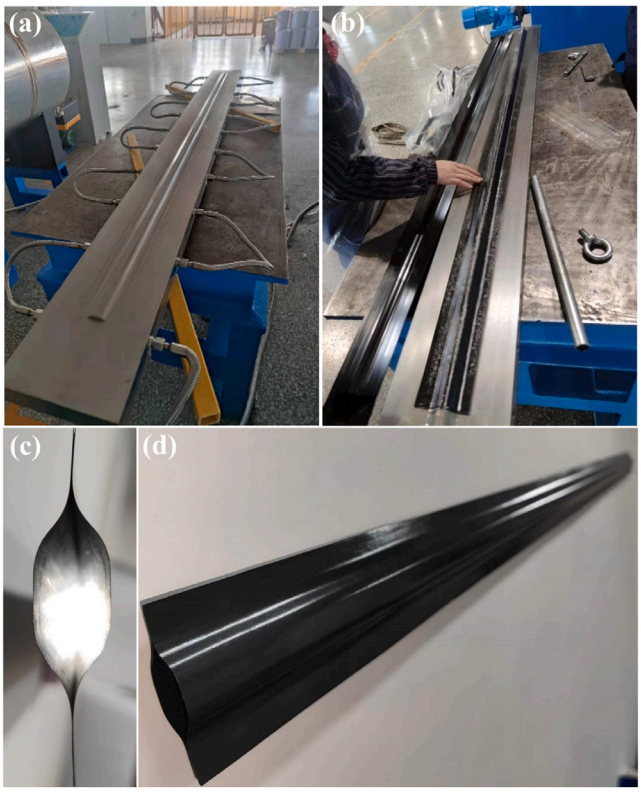

Fig. 2. Fabrication process of CTLT. (a) The mold is made of steel. (b) The Ω–shaped composite shell in the mold. (c) The cross-section shape of CTLT. (d) CTLT specimen.

concurrently expelling any trapped air. The Ω–shaped composite shell was then cured in an autoclave at a temperature of 135 °C for approximately 2 h. The fabrication process was completed by bonding two separately manufactured Ω–shaped shells together to form the CTLT.

2.2. Dynamic deployment testing

This section presents the experimental setup for performing the dynamic deployment tests of CTLT in a simulated zero-gravity environment. Figs. 3 and 4 show the schematic representation and pictures of the experimental setup, respectively. The central hub was made of an acrylic cylinder with a thickness of 10 mm, an outer diameter of 400 mm, and a height of 1200 mm. One end of the hub was fixed to the ground and from the hub center 16 equally distributed radial lines were generated using four laser projectors (Laser locator, Deli, China). These radial lines are used to help measure the evolution of the deployment angle during the dynamic deployment process. The other end of the hub was tied to one end of the CTLT using a homemade 3D-printed positioning fixture. The fixture contains grooves with the same lenticular cross-section shape as CTLT. The end of CTLT was carefully inserted into the fixture slots and then tightened with the help of screws and bolts, see Fig. 4a. The neutral axis of the CTLT is tangent to the hub surface.

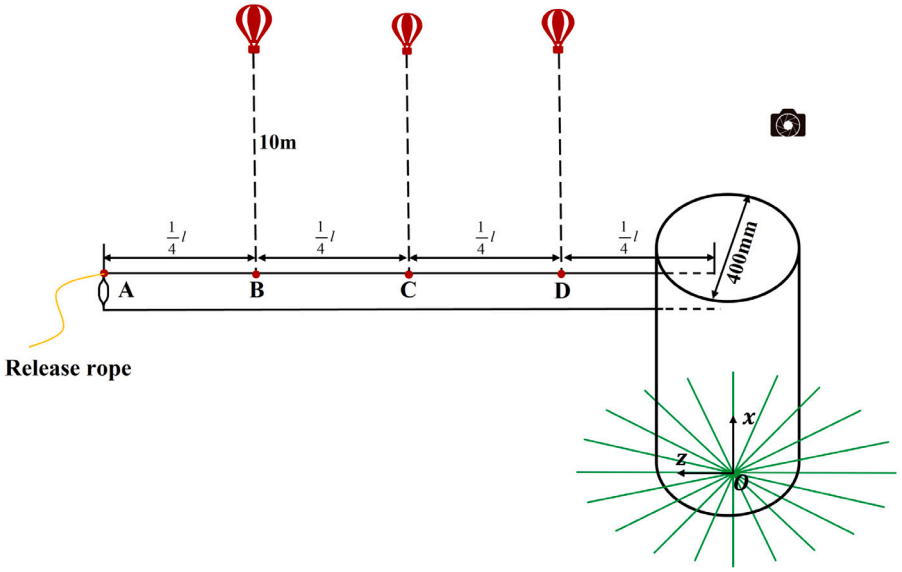

Fig. 3. Schematic representation of experimental setup for on-ground dynamic deployment testing of CTLT with the gravity compensation system.

Four small holes with a diameter of 2 mm were drilled at every quarter-length point along the longitudinal length of the CTLT (see Fig. 3 for details). Point A was connected to a rope that controls the folding and deployment of the CTLT. Points B, C, and D were connected to Helium-filled balloons with strings to compensate for the gravity of the CTLT. The He-balloons were floating in the air at a height of 10 m, and the buoyancy force at each point was measured with an electric dynamometer, see Fig. 4b. The He-balloons were expected to move synchronously with their corresponding points during the deployment of CTLT, however, in practice the He-balloons move much slower than the CTLT due to air-drag effects. After a few trial-and-error tests, the buoyancy force at Point B was set to a little larger value than those at the other two points, and the buoyancy forces at Points B, C, and D were determined as 0.456 N, 0.339 N, and 0.356 N, respectively.

The CTLT was firstly folded and wrapped around the cylindrical hub, and fastened by the release rope. As soon as the rope was released, the CTLT was self-deployed driven by the stored strain energy. The dynamic deployment deformation of CTLT was monitored using a high-speed camera (Canon 5D) placed at a height of 4 m, see Fig. 4c. In addition, the deployment test was repeated twice by stowing the CTLT for 6 and 10.5 months at a room temperature of 20 °C and a humidity of approximately 30% to 50%. The deployment behaviors of the same CTLT before and after being stowed were compared to reveal the effects of long-term storage on the performance of CTLT.

3. Simulations

Finite element simulations were also conducted to further characterize the dynamic deployment response of the considered CTLT. The model was constructed using a commercial finite element code Abaqus/Explicit 2020. For ease of performing the folding and wrapping procedures, a couple of mechanisms were also included in the model. As shown in Fig. 5, the folding/deployment mechanisms consist of a central hub, 12 rollers, and 3 plates. The finite element model of the CTLT was constructed using the four-node reduced integral shell element (S4R). The total number of the elements was selected to be 37 120 through a mesh sensitivity study. The remaining components used for performing folding and wrapping procedures were modeled as discrete rigid bodies. The dimensions of the CTLT and the central hub are identical to those in experiments. The rollers are uniformly distributed around the circle at a distance of 3.5 mm away from the hub surface with a diameter of 20 mm. Plates 1 and 2 are placed

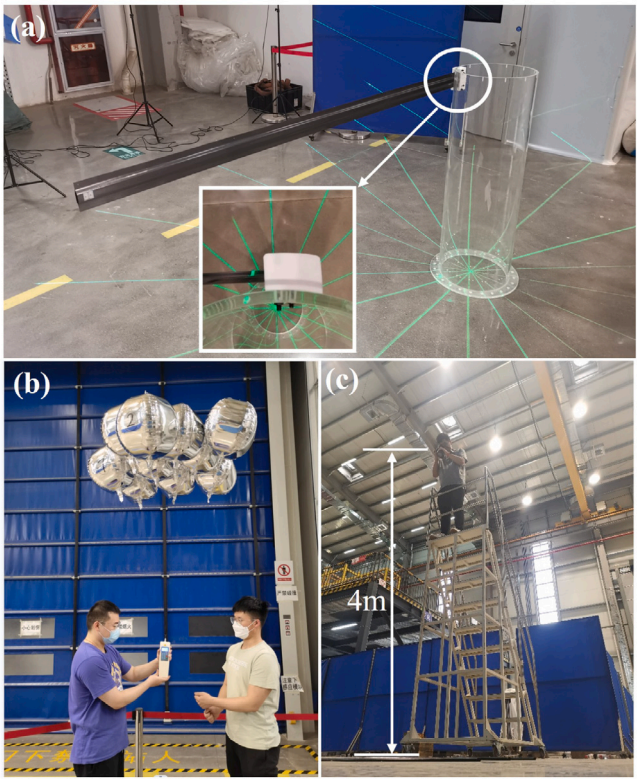

Fig. 4. Photos show the experimental setup for on-ground dynamic deployment testing of CTLT with the gravity compensation system.

symmetrically with respect to the neutral axis of CTLT and have an initial distance of 18 mm. Plate 3 is placed close to the hub surface with a tiny gap of 0.8 mm.

Fig. 6 demonstrates a three-step folding and wrapping simulation procedure for CTLT. A detailed description of the simulation setup has been given in a previous work [41]. The simulation starts by applying an 8.65 mm vertical displacement of opposite directions to Plates 1 and 2 to compress the end of the CTLT to deform it from its deployed state to a flattened state. Then, Plates 1 and 2 are removed and Plate

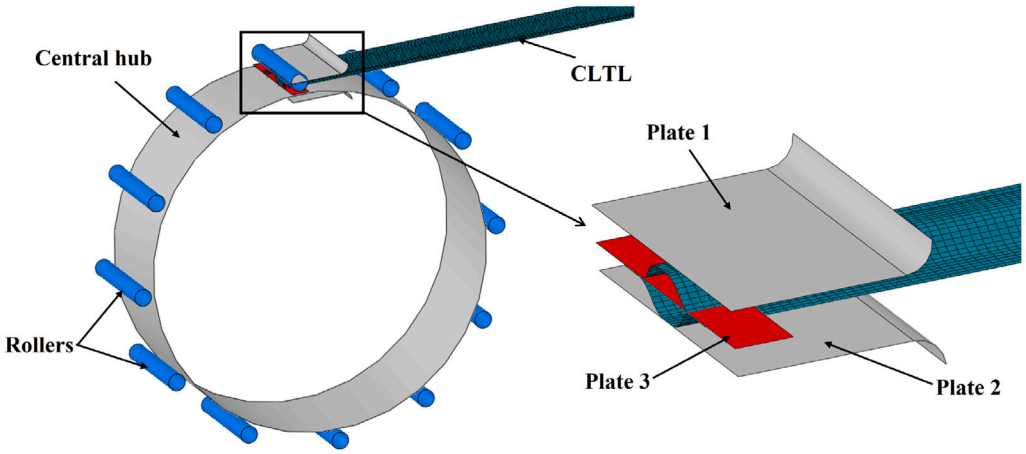

Fig. 5. Finite element model of the CTLT along with its folding/deployment mechanisms. The CTLT is modeled as a deformable composite shell structure, and the surrounding mechanisms including the central hub, rollers, and plates are all modeled as rigid bodies.

3 is activated. The flattened end of the CTLT is then fully constrained between Plate 3 and the hub surface. Next, the hub and the constraint Plate 3 are rotated 9.42 rad simultaneously, which drives the CTLT to be progressively flattened and coiled into the gap between the central hub and the guide rollers. The other end of the CTLT was restricted to moving horizontally only to make the coiling process smooth and steady. The general contact algorithm in Abaqus was utilized to deal with the complex interactions between the CTLT and various components of the folding/deployment mechanisms. Specifically, a frictional contact algorithm was applied with a coefficient of friction of 0.1 between the CTLT surfaces and Plates 1 and 2 in the first step, as well as between the CTLT surfaces and the hub and the roller surfaces in the third step. A 'no slip and no separation' condition was applied between the CTLT surfaces and Plate 3 in the second and third steps. The explicit dynamic finite element procedure (*Dynamic, Explicit in Abaqus) was employed to solve the highly nonlinear folding and coiling deformation of CTLT, as well as the complicated contact problems in the process. The step time periods of the three steps were set to 0.4, 0.4, and 8.0 s, respectively. Quasi-static conditions were ensured by monitoring the kinetic energy of CTLT being a small value, less than 5% of the strain energy of CTLT throughout most of the folding and wrapping process, and therefore during this process, almost all of the external work is converted into the strain energy stored in the deformation of CTLT. The Tsai–Hill failure criterion was employed for failure analysis [42].

The CTLT was firstly folded and wrapped around the hub and then stowed in the coiled state for a prolonged period of time to be finally deployed on demand. The strain energy relaxation caused by the long-term storage was simulated by inducing a change in the material properties as given in Table 3. This was achieved by specifying a change in the virtual temperature before performing the deployment simulation. The final deployment simulation was performed as a true transient analysis using the same explicit dynamic solver. All the restrictions were removed except for the constraint of Plate 3, and the CTLT was deployed freely. In addition, in order to simulate the effect of air resistance during the free deployment, a constant viscous pressure load with a coefficient of 6E−9 was applied to the top and bottom surfaces of the CTLT.

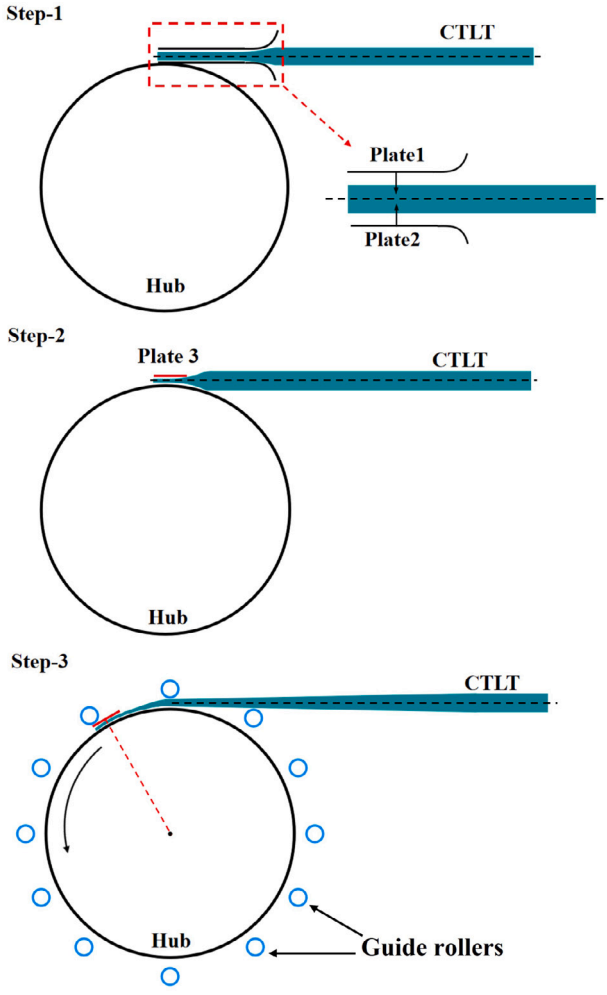

Fig. 6. Schematic of the folding and wrapping process of CTLT. Step-1: The end of CTLT is flattened by moving Plates 1 and 2 closer together. Step-2: Plates 1 and 2 are removed and Plate 3 is activated to constrain the flattened end of CTLT. Step-3: The central hub and Plate 3 are rotated simultaneously to drive the CTLT to be progressively flattened and coiled into the gap between the hub and guide rollers.

4. Results

4.1. Coiling behavior

Fig. 7 gives the folding and coiling behavior analysis results of CTLT. It is shown from Fig. 7a that the strain energy stored in the CTLT increases slightly as the end of CTLT is flattened in the flattening process of *Step-1*, and then remains almost unchanged in *Step-2* to change the contact conditions, and then increases smoothly up to about 8.46 J in the wrapping process of *Step-3*. The kinetic energy of CTLT

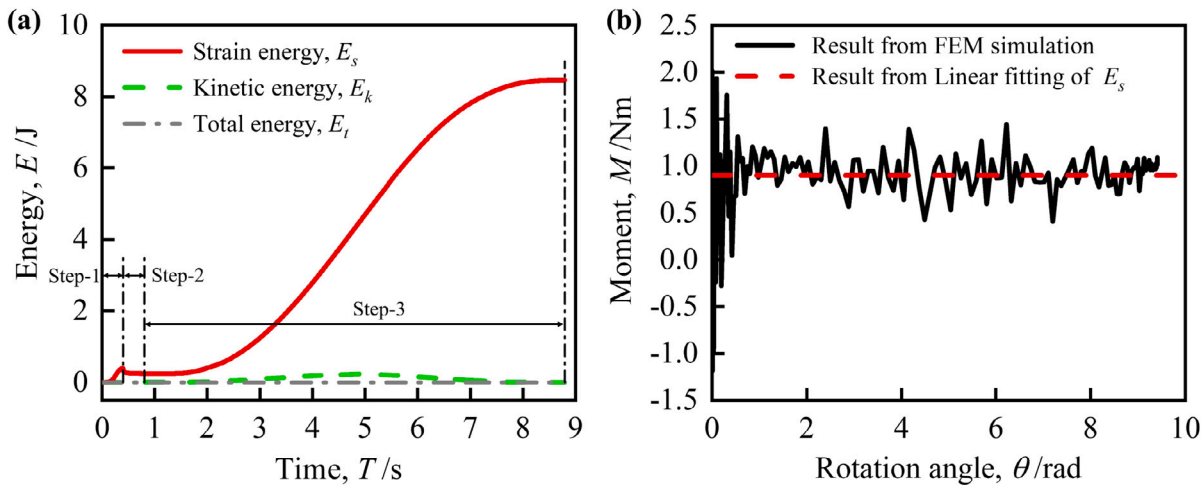

Fig. 7. Simulation results of coiling process. (a) Variation of strain energy of CTLT during the quasi-static flattening and coiling process. (b) Rotational moment as a function of the rotational angle.

is negligible compared to the strain energy throughout the complete process of folding and wrapping as expected. Fig. 7b gives the evolution of the rotational moment as a function of the rotational angle of the central hub in the wrapping process. It shows that the rotational moment increases rapidly within the initial small deformation range with the increase of the rotational angle and then quickly reaches a stable level of 0.9 N m. This prediction agrees qualitatively well with the experimental observations given in [18,20] as well as the theoretical and numerical predictions given in [41,43]. The fluctuations in the rotational moment–angle curve are understandable since the quasi-static simulation was performed using a true dynamic finite element procedure [44]. Fig. 8 shows the distribution of the Tsai–Hill failure index in the deformed configurations of the CTLT at various stages in the flattening and coiling process. The Tsai–Hill failure index of the CTLT remains less than 1.0 which indicates no failure occurrence.

4.2. Deployment behavior

A typical set of snapshots of the CTLT in the dynamic deployment process are presented in Fig. 9 and comparisons are made between experimental observations and numerical predictions. The simulation captures the overall deployment behavior observed in the experiments fairly well. As soon as the deployment is activated, either by experimentally releasing the rope or by numerically removing the guide rollers, the CTLT is deployed immediately; one end of the CTLT is attached to the hub and the other end moves quickly showing a spiral trajectory. The results show that it takes about 5.70 s for the CTLT to be self-deployed from its fully coiled state to a fully deployed state. Note that the CTLT is coiled around the hub for 1.5 circles before being deployed. In the simulations, the CTLT is deployed layer by layer, while in the experiments the CTLT stopped its deployment and instead unwound and expanded radially at a certain point. This is referred to as the blossoming effect. The observed discrepancy between simulation and experiment is likely attributed to the unintended movement of the He-balloons within the gravity unloading system. The air resistance effect hindered perfect synchronicity between the motion of the CTLT and the He-balloons. It is worth noting that in addition to the dynamic deployment method discussed in the paper, there exists an alternative controlled deployment method for deploying the CTLT. It involves rotating the central hub, which facilitates a controlled path and speed of deployment. The difference between the two deployment methods has been addressed with FE simulations in a previous work [41]. Moreover, although a few studies have been devoted to understanding the blossoming effects of individual deployable booms [45–47], in practical space applications, the CTLTs undergo concurrent deployment deformation associated with membranes such as solar sails or antenna reflectors, leading to a more complex deployment scenario, which remains yet unexplored.

Fig. 10a illustrates the path of the free end of CTLT during deployment which clearly follows a spiral trajectory. The deployment behavior of CTLT is quantified by the parameter "deployment angle" α, which is calculated by the angle between the current orientation and the initial orientation of the tangent line at the free end of CTLT as illustrated in Fig. 10a. Fig. 10b shows the evolution of the deployment angle α as a function of the deployment time T. The simulation results agree very well with the experimental data and indicate that the CTLT is deployed quickly at the initial stage of the deployment where the deployment angle increases rapidly with time, and then the deployment angle of CTLT increases slowly with further increasing time. Namely, the deployment speed of the CTLT gradually decreases with the deployment time. This can be interpreted from the energy consumption point of view. As has been discussed above, the dynamic deployment of CTLT is driven by releasing the strain energy stored in its folded deformation. Specifically, the strain energy stored in the structure E_s is transformed into two forms, i.e., the viscous dissipated energy E_v and the kinetic energy E_k. The energy balance, which is referred to as the total energy of the model E_{total} in Abaqus, is then defined as $E_{total} = E_s - E_v - E_k$. Fig. 11 presents the variation of these model energies as a function of the deployment time. It is shown that (*i*) the total energy E_{total} remains always zero at all times which gives an indication of the accuracy of the computation; and (*ii*), at the initial stage of the deployment from the initiation to about 0.72 s, the kinetic energy of the structure is larger than the energy dissipated by viscous pressure, which means that more of the released strain energy has been transformed into kinetic energy of the structure in this stage; on the contrast, in the later stage of the deployment (deployment time $T > 0.72$ s), more of the released strain energy is dissipated by viscous pressure. As a consequence, the kinetic energy of the structure (see the green dashed line in Fig. 11) increases gradually and peaks at 0.54 s and then decreases with the increase of deployment time, and this is the reason why the CTLT is deployed quickly at the initial stage but slowly at the later stage of the deployment.

4.3. Effect of long-term storage

Finally, we move on to investigate the long-term storage effect on the dynamic deployment behavior for CTLT. First, we use simulations to explore the effect of different levels of modulus reduction due to the viscoelastic behavior of the composite materials. As has been discussed in Section 2.1 and Table 3, five hypothetical cases are generated by

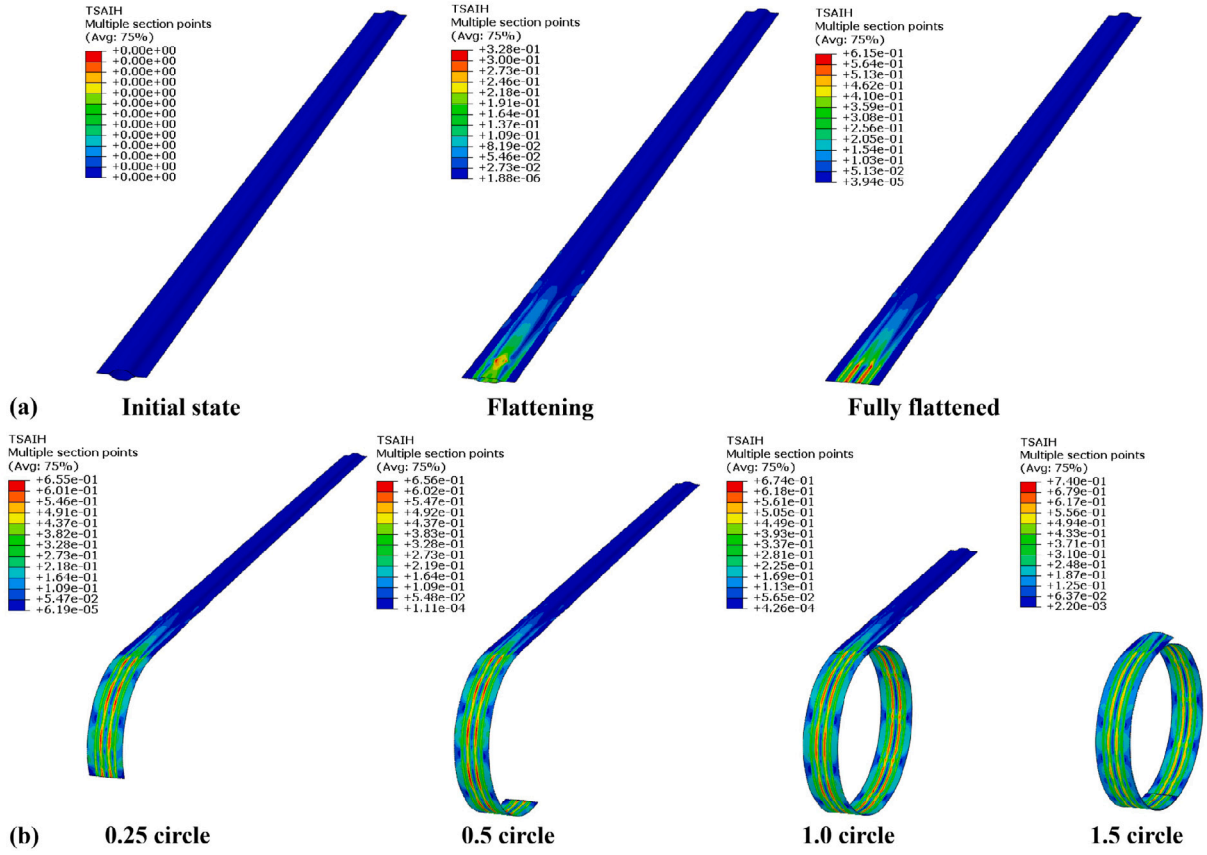

Fig. 8. Distribution of Tsai–Hill failure index in the deformed configuration of CTLT at various stages in the (a) flattening and (b) coiling process.

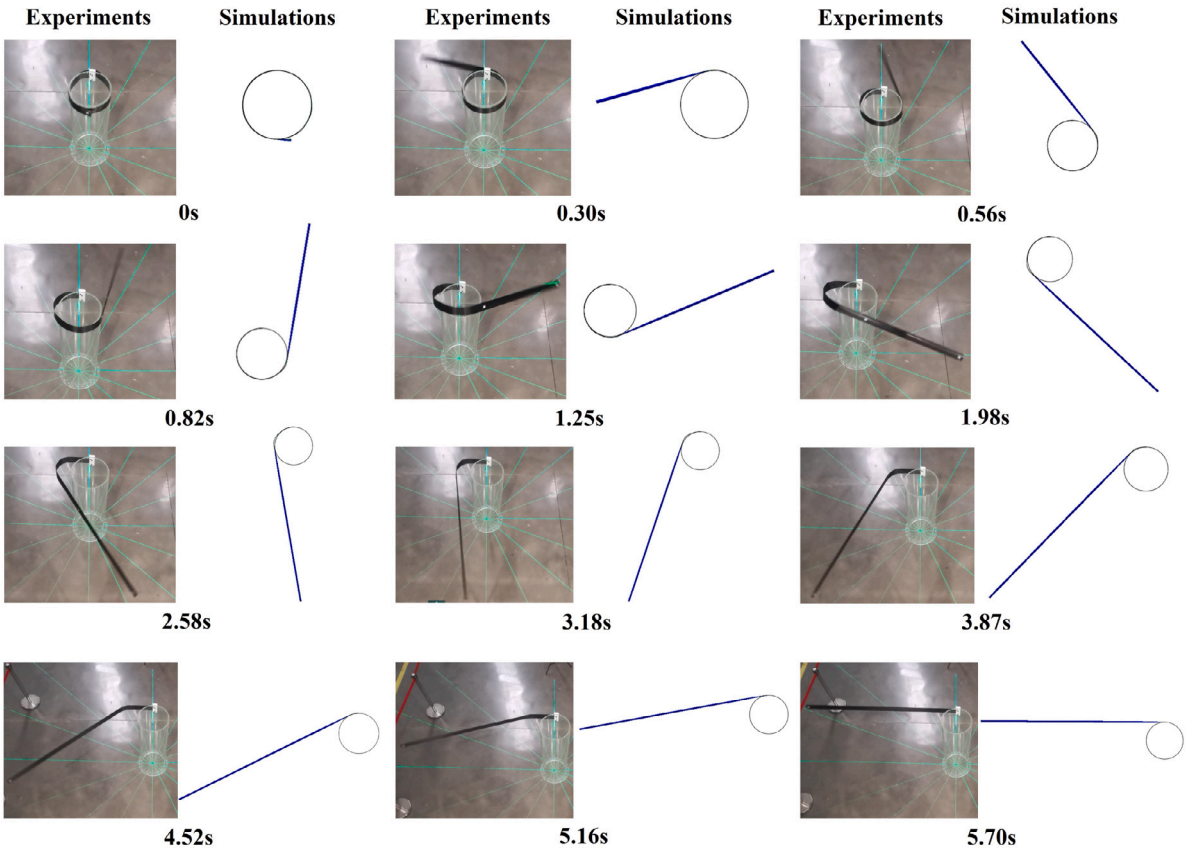

Fig. 9. Deployment snapshots of the CTLT at different phases from experiments and simulations.

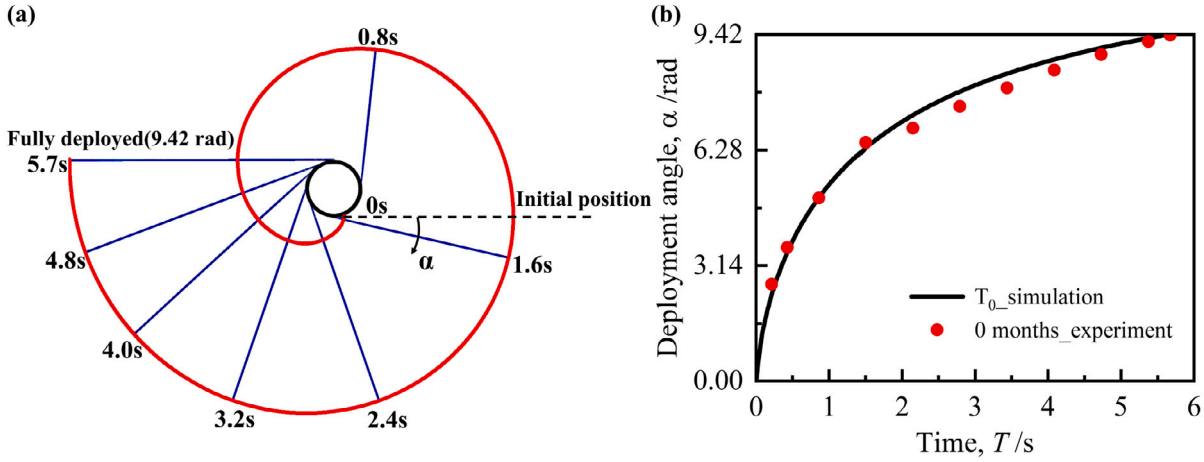

Fig. 10. Dynamic deployment behavior of the CTLT. (a) The free end of the CTLT moves showing a spiral trajectory, and the deployment angle α is defined by calculating the included angle between the current and the initial orientation of the tangent line at the free end of CTLT. (b) Evolution of the deployment angle as a function of the deployment time. The blue solid line denotes simulation results and the red dots denote experimental data. (For interpretation of the references to color in this figure legend, the reader is referred to the web version of this article.)

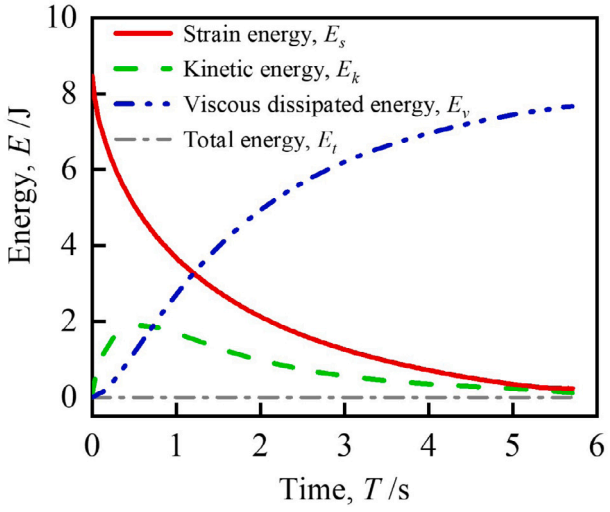

Fig. 11. Energy histories of the CTLT in the dynamic deployment process.

considering the epoxy matrix had a modulus reduction of 10%, 20%, 30%, 40%, and 50% from the initial value. The simulation predicted deployment angle versus time curves for these hypothetical cases are visualized in the form of a heatmap in Fig. 12a. It suggests that the deployment process takes longer to be completed for the case with a larger reduction in matrix modulus. The experimental data are also presented in Fig. 12a as markers, where solid blue dots indicate immediate deployment without stowage, and green squares and red triangles represent CTLT deployment after being stowed for 6 and 10.5 months, respectively. By correlating the experimental data with the simulations, we find that storing the CTLT for 6 and 10.5 months results in a reduction of approximately 20% and 30% reduction in the modulus of the epoxy matrix, respectively. Fig. 12b shows the reduction in the stored strain energy as a result of long-term storage and epoxy matrix modulus relaxation. Briefly, longer storage of the CTLT leads to a larger reduction in the modulus of the epoxy matrix, resulting in a decrease in the stored strain energy and a slower deployment speed, see Table 4 for a summary.

Permanent deformation can also occur as a result of long-term storage for space deployable structures made of fiber-reinforced epoxy composite laminates [32,48]. The design of CTLT should ensure that the materials do not experience permanent deformation during folding

Table 4
Deployment behavior after long-term storage.

Storage time (Virtural temperature)	Deployment time (Experiment)	Deployment time (Simulation)	Stored strain energy (Simulation)
Initial state/T_0	5.72 s	5.70 s	8.46 J
6 months/T_2	6.19 s	6.31 s	7.67 J
10.5 months/T_3	6.58 s	6.75 s	7.23 J

Table 5
Permanent shape change in the CTLT after being stowed for 6 and 10.5 months compared to its initial state.

Storage time	Deflection/mm	Width of cross-section/mm	Height of cross-section/mm
Initial state	0	16.04	81.56
6 months	25.18	14.91	83.25
10.5 months	44.02	13.39	84.19

and stowage. Nevertheless, long-term storage may result in the accumulation of plastic strains in the epoxy matrix, which can lead to a permanent shape change in the CTLT. Fig. 13 presents the experimentally observed permanent shape change in the CTLT after being stowed for 6 and 10.5 months. It has been shown that an extended storage period leads to an increase in the permanent deformation of CTLT. To be specific, storing the CTLT for 6 and 10.5 years results in a lateral deflection of 25.18 mm and 44.02 mm, respectively. Furthermore, long-term storage also causes a permanent shape change in the cross-section of CTLT, as shown in the inserted plots in Fig. 13. The lenticular cross-section becomes elongated in height while being short in width, hence, it becomes flatter compared to the initial state. The size changes in the geometry of CTLT are summarized in Table 5. The change in the cross-section of CTLT is expected to alter its bending stiffness, with an increase in the bending stiffness about the x-axis and a decrease about the y-axis as per our previous study [49]. The permanent deformation of the CTLTs will undoubtedly have an impact on the surface accuracy of space deployable structures that rely on them for support, such as the wrapped-rib antennas. However, to the best of our knowledge, the underlying mechanics that lead to accumulated permanent deformation during the long-term storage of composite space deployable structures have not been investigated yet. In the future, a visco-plastic multiscale material model should be utilized to address this issue.

5. Discussion and conclusion

CTLT has great potential as a promising self-deployable boom for the construction of large-scale space deployable mechanisms. Due to

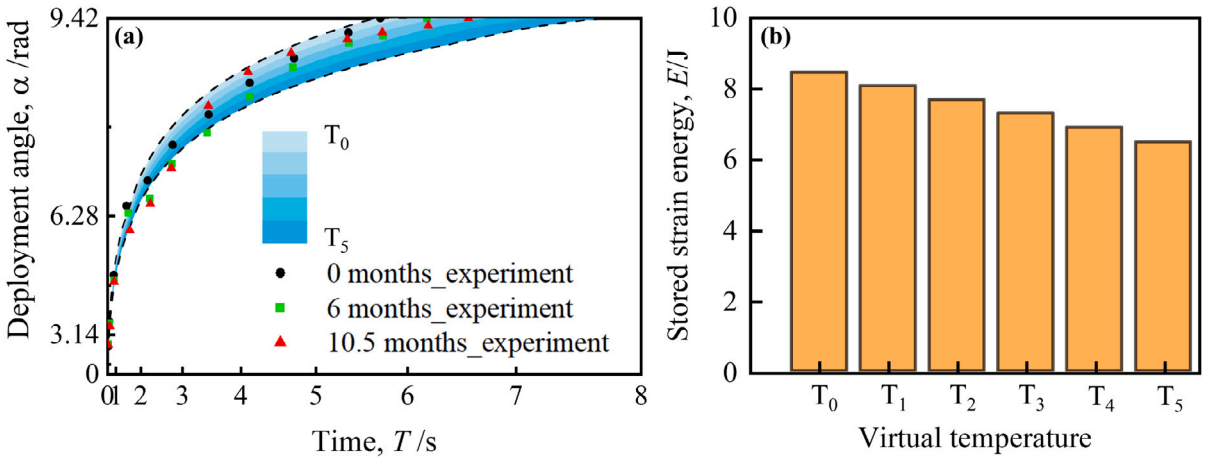

Fig. 12. Effect of long-term storage on the deployment behavior of CTLT. (a) Evolution of the deployment angle with time during dynamic deployment of CTLTs after being stowed for a given period of time. The simulation results are visualized in the form of a heatmap, with deeper color indicating longer storage durations. The experimental data is represented using a variety of markers, with solid blue dots indicating immediate deployment without stowage, and green squares and red triangles representing CTLT deployment after being stowed for 6 and 10.5 months, respectively. (b) The simulation results also demonstrate that storing the CTLT for an extended period leads to a reduction in its stored strain energy. (For interpretation of the references to color in this figure legend, the reader is referred to the web version of this article.)

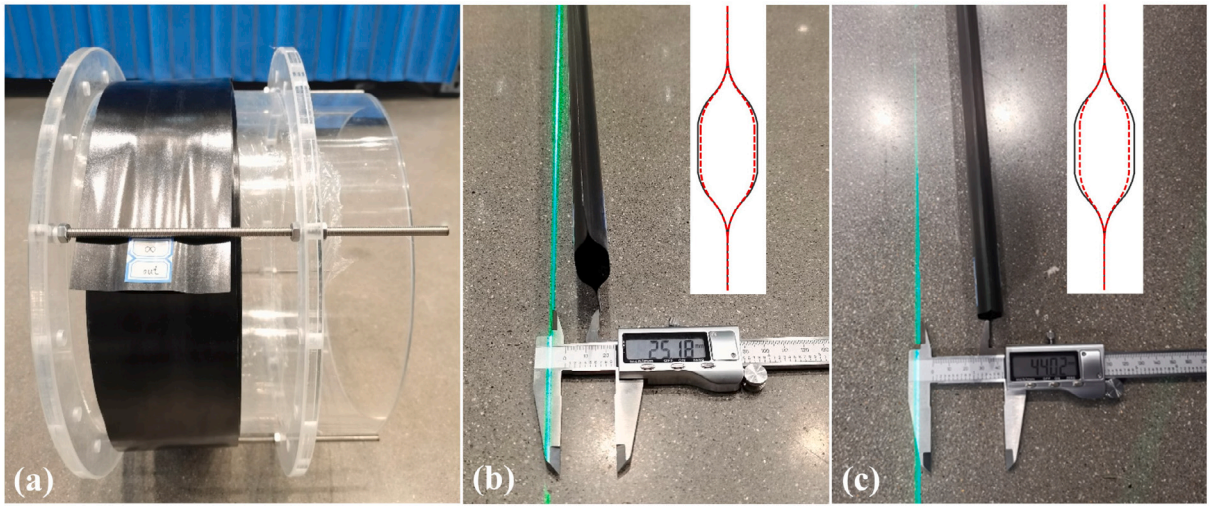

Fig. 13. Permanent shape change in the CTLT after being stowed for an extended period. (a) Stowage configuration of the CTLT. (b) and (c) Permanent lateral deflection of the CTLT after being stowed for 6 and 10.5 months, respectively. The inserted plots at the up-right corner illustrate the permanent shape change in the cross-section of the CTLT.

the limited volume of satellites, CTLTs often need to be folded and stored for extended periods before being deployed into their operational configuration. Understanding the folding, stowage, and deployment behaviors of CTLT is crucial for its structural design. To this end, there are two primary challenges to overcome. The first challenge involves developing an effective gravity compensation system that can be used for performing on-ground dynamic deployment tests of CTLT. This is a non-trivial task because the CTLT undergoes significant shape changes in a very short period of deployment, which makes it difficult to maintain a consistent and stable testing environment. The second challenge is to analyze the strain energy relaxation in CTLT during extended periods of storage. This analysis is critical to comprehending the impact of long-term storage on the deployment performance of CTLT.

To tackle the above-mentioned challenges, this paper presents a combination of experimental and numerical studies. The experimental study involves the manufacture of a two-meter-long CTLT prototype, the design and construction of a gravity compensation system, and the on-ground deployment testing of the prototype before and after extended storage periods. The numerical study utilizes a high-fidelity finite element model, which includes the CTLT and the folding/deployment mechanisms, to perform complete folding and deployment analyses. Additionally, the effect of long-term storage on the deployment performance is accounted for by employing a previously developed viscoelastic composite model. The experimental and numerical snapshots of the CTLT in the dynamic deployment process are presented and compared, along with the deployment angle versus time curves, and a good quantitative agreement was obtained between them. The results suggest that the CTLT undergoes rapid deployment during the initial stage, followed by a slower deployment during the latter stage. The impact of long-term storage on the performance of CTLT is manifested primarily in two aspects. Firstly, stowing the CTLT for a longer storage period results in a slower deployment speed and a longer deployment time. This effect has been accurately modeled using a previously established viscoelastic material model for fiber-reinforced composite laminates. Secondly, the experimental measurements indicate that during long-term storage, the CTLT undergoes irreversible deformation in the later deflection as well as permanent shape changes in its cross-sectional geometry. This effect is attributed to the accumulation of plastic strains in the epoxy matrix over the extended storage period. It is anticipated that a multiscale visco-plastic model

for composite materials and structures will be proposed to address this phenomenon in near future.

In the end, we would like to note that, although our work has been focused on CTLT, the experimental and numerical methods proposed here are readily applicable to the performance analysis of other kinds of thin-walled rollable and deployable booms. We hope our effects provide insights into the basic understanding of folding, stowage, and deployment behaviors of thin-ply composite laminates and deployable structures for space applications.

Declaration of competing interest

The authors declare that they have no known competing financial interests or personal relationships that could have appeared to influence the work reported in this paper.

Data availability

The Abaqus scripts used for the numerical analyses that support the findings are available to download from https://github.com/XJTU-Zhou-group/CTLT-Dynamic-Deployment.

Acknowledgments

This research was co-supported by the National Natural Science Foundation of China (grants 11972277 and 12202295), the Fundamental Research Funds for the Central Universities, People's Republic of China (No. YJ2021137), the Open Project of State Key Laboratory for Strength and Vibration of Mechanical Structures, Xi'an Jiaotong University, People's Republic of China (No. SV2021-KF-04), and the Open Project of State Key Laboratory of Structural Analysis for Industrial Equipment, Dalian University of Technology, People's Republic of China (No. GZ22120).

References

[1] Z.-Q. Liu, H. Qiu, X. Li, S.-L. Yang, Review of large spacecraft deployable membrane antenna structures, Chin. J. Mech. Eng. 30 (6) (2017) 1447–1459.
[2] X. Ma, T. Li, J. Ma, Z. Wang, C. Shi, S. Zheng, Q. Cui, X. Li, F. Liu, H. Guo, et al., Recent advances in space-deployable structures in China, Engineering (2022).
[3] J.M. Fernandez, L. Visagie, M. Schenk, O.R. Stohlman, G.S. Aglietti, V.J. Lappas, S. Erb, Design and development of a gossamer sail system for deorbiting in low earth orbit, Acta Astronaut. 103 (2014) 204–225.
[4] J.M. Fernandez, G.K. Rose, C.J. Younger, G.D. Dean, J.E. Warren, O.R. Stohlman, W.K. Wilkie, NASA's advanced solar sail propulsion system for low-cost deep space exploration and science missions that use high performance rollable composite booms, in: International Symposium on Solar Sailing, Vol. NF1676L-25177, 2017.
[5] J. Liu, P. Zhao, C. Wu, K. Chen, W. Ren, L. Liu, Y. Tang, C. Ji, X. Sang, SIASAIL-I solar sail: from system design to on-orbit demonstration mission, Acta Astronaut. 192 (2022) 133–142.
[6] W.K. Wilkie, Overview of the NASA advanced composite solar sail system (ACS3) technology demonstration project, in: AIAA Scitech 2021 Forum, 2021, p. 1260.
[7] J. Block, M. Straubel, M. Wiedemann, Ultralight deployable booms for solar sails and other large gossamer structures in space, Acta Astronaut. 68 (7–8) (2011) 984–992.
[8] M. Straubel, J. Block, M. Sinapius, C. Hühne, Deployable composite booms for various gossamer space structures, in: 52nd AIAA/ASME/ASCE/AHS/ASC Structures, Structural Dynamics and Materials Conference 19th AIAA/ASME/AHS Adaptive Structures Conference 13t, 2011, p. 2023.
[9] K.N. Urata, J.T.S. Sumantyo, C.E. Santosa, T. Viscor, A compact C-band CP-SAR microsatellite antenna for earth observation, Acta Astronaut. 159 (2019) 517–526.
[10] A. Tresoldi, J. Shore, A.C. Austin, G.S. Aglietti, Development of a deployable Synthetic Aperture Radar antenna for a nanosatellite conceptual design, Acta Astronaut. (2023).
[11] K.N. Urata, J.T. Sri Sumantyo, C.E. Santosa, T. Viscor, Development of an L-band SAR microsatellite antenna for earth observation, Aerospace 5 (4) (2018) 128.
[12] A. da Silva Curiel, P. Whittaker, R. Bird, A. Haslehurst, P. Nejadi, I. Victoria, A. Cawthorne, C. Underwood, M. Sweeting, Synthetic Aperture Radar on a nanosatellite-is it possible? in: Proceedings of the 12th IAA Symposium on Small Satellites for Earth Observation, International Academy of Astronautics (IAA), 2019.
[13] O. Yoshiro, J. Reveles, V. Fraux, D.-J. Ashley, Deployable wrapped rib assembly, 2019, US Patent App. 16/348, 390.
[14] J.-C. Angevain, A. Ihle, G. Rodrigues, J. Santiago-Prowald, Large deployable spaceborne reflector antennas in Europe: progress status and perspectives, in: 2019 13th European Conference on Antennas and Propagation (EuCAP), IEEE, 2019, pp. 1–5.
[15] R. Freeland, R. Helms, M. Mikulas, The Applicability of past innovative concepts to the technology for new extremely large space antenna/telescope structures, SAE Trans. (2006) 160–173.
[16] T.-W. Liu, J.-B. Bai, S.-L. Li, N. Fantuzzi, Large deformation and failure analysis of the corrugated flexible composite skin for morphing wing, Eng. Struct. 278 (2023) 115463.
[17] Z. Chu, Y. Lei, Design theory and dynamic analysis of a deployable boom, Mech. Mach. Theory 71 (2014) 126–141.
[18] W. Chen, G. Fang, Y. Hu, An experimental and numerical study of flattening and wrapping process of deployable composite thin-walled lenticular tubes, Thin-Walled Struct. 111 (2017) 38–47.
[19] J. Bai, J. Xiong, J. Gao, X. Yi, Analytical solutions for predicting in-plane strain and interlaminar shear stress of ultra-thin-walled lenticular collapsible composite tube in fold deformation, Compos. Struct. 97 (2013) 64–75.
[20] J.-B. Bai, D. Chen, J.-J. Xiong, R.A. Shenoi, Folding analysis for thin-walled deployable composite boom, Acta Astronaut. 159 (2019) 622–636.
[21] P. Seefeldt, P. Spietz, T. Sproewitz, J.T. Grundmann, M. Hillebrandt, C. Hobbie, M. Ruffer, M. Straubel, N. Tóth, M. Zander, Gossamer-1: Mission concept and technology for a controlled deployment of gossamer spacecraft, Adv. Space Res. 59 (1) (2017) 434–456.
[22] J.A. Firth, M.R. Pankow, Advanced dual-pull mechanism for deployable spacecraft booms, J. Spacecr. Rockets 56 (2) (2019) 569–576.
[23] J.A. Firth, M.R. Pankow, Minimal unpowered strain-energy deployment mechanism for rollable spacecraft booms: ground test, J. Spacecr. Rockets 57 (2) (2020) 346–353.
[24] N. Okuizumi, A. Watanabe, H. Ito, Efficient storage and deployment of tubular composite boom using spring root hinges, J. Spacecr. Rockets 58 (2) (2021) 334–344.
[25] M.E. Zander, M.K. Chamberlain, D. Jost, D.R. Müller, N. Hagmeister, M. Straubel, C. Hühne, Design and testing of the BionicWingSat in a zero-g flight campaign-a 2U-CubeSat with deployable, biologically-inspired wings, in: AIAA SCITECH 2023 Forum, 2023, p. 2697.
[26] T. Rybus, K. Seweryn, Planar air-bearing microgravity simulators: Review of applications, existing solutions and design parameters, Acta Astronaut. 120 (2016) 239–259.
[27] T. Takano, M. Natori, K. Miyoshi, T. Inoue, Characteristics verification of a deployable onboard antenna of 10 m maximum diameter, Acta Astronaut. 51 (11) (2002) 771–778.
[28] M. Leipold, M. Eiden, C. Garner, L. Herbeck, D. Kassing, T. Niederstadt, T. Krüger, G. Pagel, M. Rezazad, H. Rozemeijer, et al., Solar sail technology development and demonstration, Acta Astronaut. 52 (2–6) (2003) 317–326.
[29] D. Schultheiß, Gravity Compensation of Deployable Solar Arrays for Small Spacecraft (Ph.D. thesis), University of Cambridge, 2003.
[30] H. Mallikarachchi, S. Pellegrino, Deployment dynamics of ultrathin composite booms with tape-spring hinges, J. Spacecr. Rockets 51 (2) (2014) 604–613.
[31] P. Mallol, H. Mao, G. Tibert, Experiments and simulations of the deployment of a bistable composite boom, J. Spacecr. Rockets 55 (2) (2018) 292–302.
[32] J.E. Salazar, J.M. Fernandez, Experimental characterization of the dimensional stability of deployable composite booms during stowage, in: AIAA SciTech 2021 Forum, 2021, p. 0195.
[33] B. Adamcik, J. Firth, M. Pankow, J.M. Fernandez, Impact of storage time and operational temperature on deployable composite booms, in: AIAA Scitech 2020 Forum, 2020, p. 1183.
[34] T. Tang, S.D. Felicelli, Computational evaluation of effective stress relaxation behavior of polymer composites, Int. J. Eng. Sci. 90 (2015) 76–85.
[35] X. Liu, T. Tang, W. Yu, R.B. Pipes, Multiscale modeling of viscoelastic behaviors of textile composites, Internat. J. Engrg. Sci. 130 (2018) 175–186.
[36] K. Kwok, S. Pellegrino, Micromechanics models for viscoelastic plain-weave composite tape springs, Aiaa J. 55 (1) (2017) 309–321.
[37] N. An, Q. Jia, H. Jin, X. Ma, J. Zhou, Multiscale modeling of viscoelastic behavior of unidirectional composite laminates and deployable structures, Mater. Des. 219 (2022) 110754.
[38] A. Gomez-Delrio, K. Kwok, Stowage and recovery of thin-ply composite deployable structures, in: AIAA Scitech 2020 Forum, 2020, p. 0205.
[39] W. Klimm, K. Kwok, Surface accuracy of viscoelastic composite thin-shell deployable reflector antennas, in: AIAA Scitech 2020 Forum, 2020, p. 0932.
[40] P. Fernandes, B. Sousa, R. Marques, J.M.R. Tavares, A. Marques, R.N. Jorge, R. Pinto, N. Correia, Influence of relaxation on the deployment behaviour of a cfrp composite elastic–hinge, Compos. Struct. 259 (2021) 113217.
[41] J. Deng, N. An, Q. Jia, X. Ma, Deployment analysis of composite thin-walled lenticular tubes with effect of storage time and temperature, Chin. J. Aeronaut. (2023).
[42] T.-W. Liu, J.-B. Bai, H.-T. Xi, N. Fantuzzi, G.-Y. Bu, Y. Shi, Experimental and numerical investigation on folding stable state of bistable deployable composite boom, Compos. Struct. 320 (2023) 117178.

[43] T.-W. Liu, J.-B. Bai, N. Fantuzzi, Folding behavior of the thin-walled lenticular deployable composite boom: Analytical analysis and many-objective optimization, Mech. Adv. Mater. Struct. (2022) 1–19.
[44] Q. Jia, N. An, X. Ma, J. Zhou, A dynamic finite element procedure for bending collapse of composite thin-walled lenticular tubes, Compos. Struct. (ISSN: 0263-8223) 287 (2022) 115364.
[45] A. Hoskin, A. Viquerat, G.S. Aglietti, Tip force during blossoming of coiled deployable booms, Int. J. Solids Struct. 118 (2017) 58–69.
[46] S. Wang, M. Schenk, S. Jiang, A. Viquerat, Blossoming analysis of composite deployable booms, Thin-Walled Struct. 157 (2020) 107098.
[47] S. Wang, M. Schenk, H. Guo, A. Viquerat, Tip force and pressure distribution analysis of a deployable boom during blossoming, Int. J. Solids Struct. 193 (2020) 141–151.
[48] M.M. Yapa Hamillage, W.J. Klimm, K. Kwok, Permanent shape change of thin-ply composites, in: AIAA SCITECH 2022 Forum, 2022, p. 1117.
[49] Q. Jia, N. An, X. Ma, J. Zhou, Exploring the design space for nonlinear buckling of composite thin-walled lenticular tubes under pure bending, Int. J. Mech. Sci. (ISSN: 0020-7403) 207 (2021) 106661.